analytical chemistry

Article

pubs.acs.org/ac

Label-Free SERS Selective Detection of Dopamine and Serotonin Using Graphene-Au Nanopyramid Heterostructure

Pu Wang,[†] Ming Xia,[†] Owen Liang,[†] Ke Sun,[†,‡] Aaron F. Cipriano,[§] Thomas Schroeder,[∥] Huinan Liu,[§] and Ya-Hong Xie*[,†]

[†]Department of Materials Science and Engineering and California Nano Systems Institute, University of California, Los Angeles, Los Angeles, California 90095-1595, United States

[‡]WaferTech, LLC, 5509 NW Parker St., Camas, Washington 98607, United States

[§]Department of Bioengineering, Materials Science and Engineering Program, University of California at Riverside, Riverside, California 92521, United States

[∥]Innovations for High Performance (IHP), Im Technologiepark 25, Frankfurt (Oder) D-15236, Germany

Supporting Information

ABSTRACT: Ultrasensitive detection and spatially resolved mapping of neurotransmitters, dopamine and serotonin, are critical to facilitate understanding brain functions and investigate the information processing in neural networks. In this work, we demonstrated single molecule detection of dopamine and serotonin using a graphene−Au nanopyramid heterostructure platform. The quasi-periodic Au structure boosts high-density and high-homogeneity hotspots resulting in ultrahigh sensitivity with a surface enhanced Raman spectroscopic (SERS) enhancement factor ~10^{10}. A single layer graphene superimposed on a Au structure not only can locate SERS hot spots but also modify the surface chemistry to realize selective enhancement Raman yield. Dopamine and serotonin could be detected and distinguished from each other at 10^{-10} M level in 1 s data acquisition time without any pretreatment and labeling process. Moreover, the heterostructure realized nanomolar detection of neurotransmitters in the presence of simulated body fluids. These findings represent a step forward in enabling in-depth studies of neurological processes including those closely related to brain activity mapping (BAM).

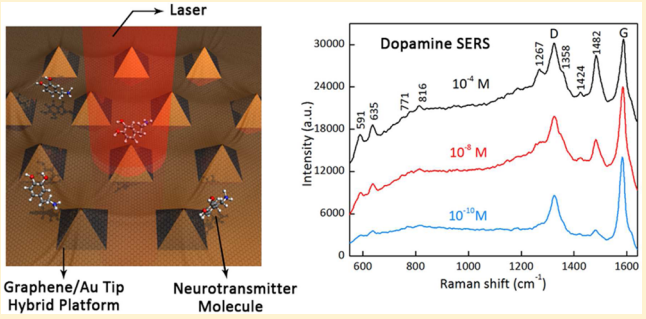

The brain activity mapping (BAM) project has set goals in developing tools to not only measure the activity of neurons in brain circuits but also to analyze and model the brain circuits.[1] Tools capable of providing spatial and temporal profiles of neurotransmitters in vivo will be ultimately required. Sensitive detection of neurotransmitters is the cornerstone for advancing the understanding of neurological processes.[2] Dopamine and serotonin, which regulate numerous biological processes, are the most humanly important neurotransmitters.[3] Dopamine deficiency causes major clinical symptoms of Parkinson's disease (PD).[4] Recent research indicates that serotonin also plays a crucial role in PD, especially in PD treatment.[5,6]

The detection of these two neurotransmitters especially serotonin remains challenging mainly due to their low basal concentrations in the vicinity of neuronal junctions (10^{-9} to 10^{-6} M).[7] The voltammetric method gains its popularity in detecting oxidizable biogenic amines.[8] However, its application is restricted in two aspects: (1) It has been difficult to monitor more than one neurotransmitter at a time and (2) the detection of certain neurotransmitter in the presence of other components of body fluid (ascorbic acid, etc.) is hard to achieve due to overlapping voltammetric responses.[9,10] Surface enhanced raman spectroscopy (SERS) has been shown to be one of the effective alternatives in neurotransmitter sensing.[11,12]

The application of SERS via plasmonic nanostructures spans analytical chemistry and materials science to biological sensing and imaging.[13,14] Various metallic nanostructures with tunable plasmonic properties have been widely explored as excellent SERS active systems.[15] Investigations of single molecules by Raman spectroscopy can be achieved with a concentrated electromagnetic (EM) field at nanometer-scale hot spots. In typical SERS active systems using metallic nanoparticles, these hot spots are sparse and randomly distributed, leading to the rarity of coincidence of molecules and hotspots in highly diluted solutions. Only a very small fraction of the molecules ends up within nanometers range to individual hot spots as is required for producing measurable Raman signals. Successful detection of molecules is at the expense of long time of up to hours spent on searching for measurable signals making the technique prohibitive for practical applications, especially real-time

Received: April 25, 2015
Accepted: September 18, 2015
Published: September 18, 2015

DOI: 10.1021/acs.analchem.5b01560
Anal. Chem. 2015, 87, 10255−10261

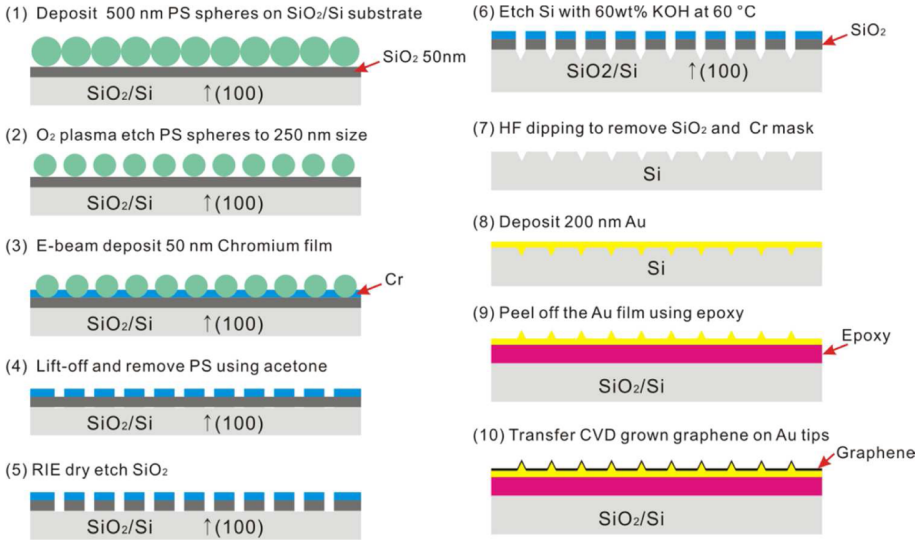

Figure 1. Schematic illustration of the graphene−Au tip hybrid platform fabrication process.

measurements. The commonly used metallic nanoparticles suffer from the shortcomings of easy degradation, limited biocompatibility and poor reproducibility. One of the labeling processes is typically introduced by covalently attaching extrinsic Raman labels to nanoparticles. The signals detected are from SERS probes via biomolecule-ligand recognition instead of biomolecules themselves. The label-based indirect SERS method suffers from a false positive issue as well as synthetic challenges.[13,16]

Here we report a novel SERS platform consisting of gold nanopyramid (referred to Au tips) structures boasting high densities of hot spots with the highest SERS enhancement factor of over 10^{10}. The structure with tips of subnanometer radius of curvature is fabricated using top-down approach and is amenable to mass production. The two-dimensional periodic nature leads to incident-laser-polarization-dependent hotspots. The structure's potential in biosensing is significantly improved by superimposing a monolayer of graphene on Au tips. The hybrid SERS platform described boasts three unique features compared to the more conventional plasmonic structures. First, the monolayer van der Waals material (vdW) such as graphene protects the metallic structure from degeneration due to the commonly encountered chemical reaction such as oxidation. It has been shown that the Raman enhancement factor of the commonly used Ag nanoparticles degrades by over 50% in a couple of weeks.[17] In contrast, the graphene based heterostructure keeps almost 100% of the sensitivity for years (see the Supporting Information). Second, the Raman peaks of graphene serve as a gauge of the near-field EM-field intensity allowing for quantitative measurement of target molecules to be obtained. Third, chemical interaction between graphene and target molecules results in selective enhancement and/or prohibition of certain SERS modes.[18] The unique feature of biochemical finger-printing of Raman spectroscopy, which greatly reduces false-positive detection combined with the capability of quantitative measurement makes the hybrid SERS platform a rare and very powerful experimental technique in biomedical research and clinical applications especially for brain activity mapping. We show in this work that the graphene-Au tip hybrid platform is capable of detecting dopamine and serotonin at 10^{-9} M level in simulated body fluids supplemented with background serum proteins with the lowest detectable molecular concentration reaching 10^{-10} M in deionized water. It sets the stage for not only in vitro applications but potentially in vivo monitoring of neurological processes including brain activities.

EXPERIMENTAL SECTION

The fabrication process of graphene-Au tip hybrid platform is shown in Figure 1. The fabrication can be divided into two major parts. The first one is to prepare Au nanopyramids, and the second one is to transfer graphene on the surface of Au nanopyramids.

Au Nanopyramids Fabrication. The Au nanopyramid fabrication is based on sphere-lithography.[19] First, polystyrene (PS) nanospheres (500 nm in diameter, Alfa Aesar) were coated on SiO_2 (50 nm)/Si wafer using scooping transfer method.[20] Before coating PS spheres, SiO_2/Si wafer was washed by Piranha solution (H_2SO_4:H_2O_2 = 3:1(volume ratio)) for 1 h at 70 °C followed by deionized water (DI water) rinsing for 3 times. In the scooping transfer process, a few drops of the diluted PS sphere suspension (5% aqueous PS sphere suspension mixed with an equal volume of ethanol) were introduced on the water surface using the partially immersed glass slide (2 cm × 10 cm). The glass slide was pretreated by a piranha solution for 1 h at 70 °C and then rinsed by DI water for 3 times. After introducing PS spheres on the water surface, PS spheres would self-assembly and form closed-packed monolayers with hexagonal patterns. When about 80% of the water surface was covered with PS spheres, PS monolayer was then transferred on SiO_2/Si substrates using simple scooping transfer method. Figure 2a shows the SEM image of the PS spheres coated on SiO_2/Si substrate. The PS spheres/SiO_2/Si sample was then dry-etched by O_2 plasma (200 W power, 50 s) to reduce the size of PS sphere to about 250 nm (Figure 2b).

After etching PS spheres, a 50 nm Cr film was deposited on the as-prepared sample using E-beam deposition (Figure 1 step (3)). The PS spheres were then lifted off by ultrasonicating the sample in acetone for 20 min, followed by DI water rinsing for 3 times. Figure 2c shows the SEM image of the sample after PS lift-off. Using the Cr film (with small holes in the film) as mask, the 50 nm SiO_2 film beneath the Cr film was dry-etched by Oxford Plasmalab plasma etcher (25 sccm Ar, 25 sccm CHF_3, RIE power 200 W, etch time 2 min).

After etching SiO_2, the hole pattern was transferred on SiO_2 from the Cr film. The sample was then etched in KOH aqueous

DOI: 10.1021/acs.analchem.5b01560
Anal. Chem. 2015, 87, 10255−10261

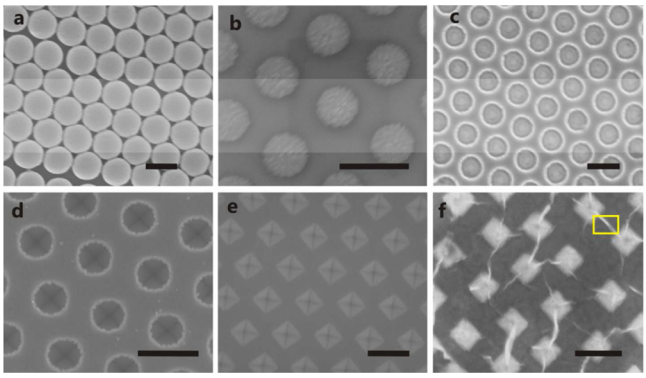

Figure 2. (a) SEM image of PS spheres on SiO_2/Si substrate. (b) SEM image of PS spheres after O_2 plasma etching for 50s. (c) SEM image of the Cr/SiO_2/Si sample after PS lift-off. (d) SEM image of the Cr/SiO2/Si sample after KOH etching. (e) SEM image of Si surface with inverse pyramidal hole. (f) SEM image of graphene transferred on Au nanopyramids. The yellow-boxed area indicates the graphene folds formed between neighboring pyramids. Scale bars in the images are 500 nm.

solution (60 wt %) for 2 min at 60 °C to form pyramidal structures on the Si surface (Figure 2d). The whole sample was then immersed into HF solution (30%) to remove SiO_2 and Cr layer. At this time, the Si pyramidal mold (Figure 2e) fabrication had been finished. 200 nm Au film was deposited on the Si mode with pyramidal structure by sputtering. 5 min epoxy was used to glue the Au film on another SiO_2 (300 nm)/Si substrate, which was used to hold the Au nanopyramids. After the epoxy cured at the room temperature, Au nanopyramids were peeled off (Figure 1 step (9)).

Graphene Transfer. Monolayer graphene was grown on copper foil by CVD method.[21] Graphene was transferred on Au nanopyramids using poly(methyl methacrylate) (PMMA) as sacrificing layer. Graphene on Cu substrates was spin-coated with PMMA layer (950 PMMA A4 from Microchem) with a spinning speed of 2000 rpm for 20 s and then was put on the surface of $CuCl_2$ solution (2M) to etch the copper. After the copper was fully etched away, PMMA with graphene layer would float on the $CuCl_2$ solution. The PMMA/graphene layer was then washed by DI water 3 times and was transferred on a Au nanopyramid substrate. After the PMMA/graphene dried, the whole sample (PMMA/graphene/Au nanopyramids) was immersed in acetone for 20 min to remove PMMA, followed by isopropanol (10 min) and DI water (10 min). The sample was then taken out from water and dried at room temperature. Figure 2f shows the SEM image of graphene transferred on Au nanopyramids. The yellow-boxed area indicates the graphene folds formed between neighboring pyramids.

Micro-Raman Spectroscopy. Micro-Raman spectra and mapping of molecules and graphene were carried out using a Renishaw inVia Raman spectroscope under ambient condition. The excitation wavelength is 633 nm from a He−Ne laser. The power of the laser was kept at 1.5 mW for single spectrum and 0.5 mW for mapping to avoid sample heating. The laser spot size was ~0.5 μm. We used a ×50 objective (numerical aperture 0.80) as well as a ×100 objective (numerical aperture 0.90). Spectral analysis was accomplished with a 1800 lines per mm grating. The spectroscope is equipped with a high speed encoded stage that enables shift of samples in XYZ directions with nominal spatial resolution of 100 nm. The spatially resolved Raman mapping data is achieved by Raman imaging with step-size down to 0.2 μm in X and Y directions with actual spatial resolution being limited by diffraction. The Raman imaging data is processed by WiRE 3.2 Raman software.

RESULTS AND DISCUSSION

The hybrid platform consists of monolayer graphene covered quasiperiodic Au nanopyramid (also referred to as Au tips) arrays shown in Figure 3. The hexagonally arranged sharp Au tips

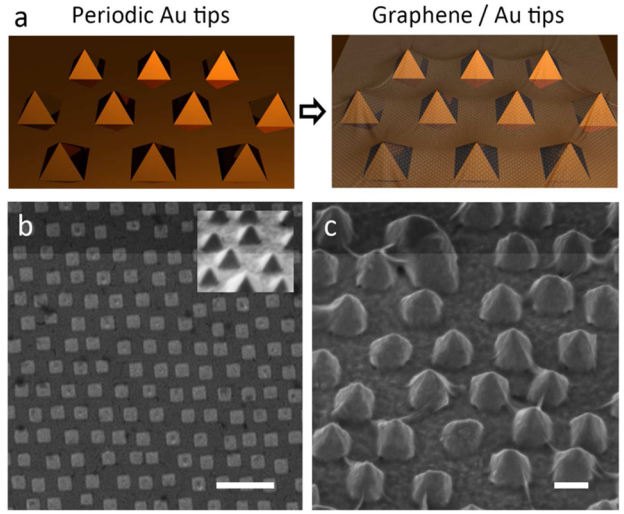

Figure 3. (a) Schematic illustration of the graphene-Au nanopyramid (tip) hybrid structure; (b) SEM image of the semiperiodic array of Au tips. Scale bar, 1 μm; (c) SEM image of hexagonally arranged arrays of Au tips covered by graphene; scale bar, 200 nm.

(radius of curvature down to 1 nm) with almost identical shape, sharpness, and orientation support markedly enhanced local fields and play a key role in the ultrahigh sensitive system. The tipped substrate can be fabricated in large scale with superior reproducibility[22] (Figure 3c).

To quantify the Raman enhancement factor of the Au tip substrate, we used the Raman spectrum of graphene as a "built-in" SERS intensity gauge. Single layer graphene is transferred on the substrate consisting of three regions located next to one another: Au tipped surface, flat Au surface, and the surface of flat SiO_2 of 300 nm thickness. Micro-Raman spectra of graphene were obtained from the three different regions using the near-resonant excitation wavelength of 633 nm (Figure 4a). Graphene Raman peaks intensity enhancement of up to 3 orders of magnitude is observed from graphene on Au tips than that on flat Au, a direct evidence of plasmon-resonance of the Au tips. Taking into consideration that within the laser illumination spot of approximately 1 μm diameter there being only one hot spot of ~10 nm × 10 nm area, SERS enhancement factor of the order of 10^{10} can be calculated. It could be seen that graphene SERS spectra taken from different spots on Au tips showed I(D) to I(G) ratios ranging from 1 to 5. Such variation originates from D band induced by 1-dimensional graphene fold.[23] The measured extinction spectrum of bare Au tipped region (Figure 4b) shows a maximum in extinction centered at 600 nm with full-width-at-half-maximum (fwhm) being ~100 nm. Various excitation wavelengths (488, 514, 633, and 785 nm) have been tested to build the relationship between plasmonic resonance and SERS enhancement (Figure 4c). Figure 4c showed the same trend in wavelength dependence, providing further evidence to the plasmonic nature of the Au tips.

DOI: 10.1021/acs.analchem.5b01560
Anal. Chem. 2015, 87, 10255−10261

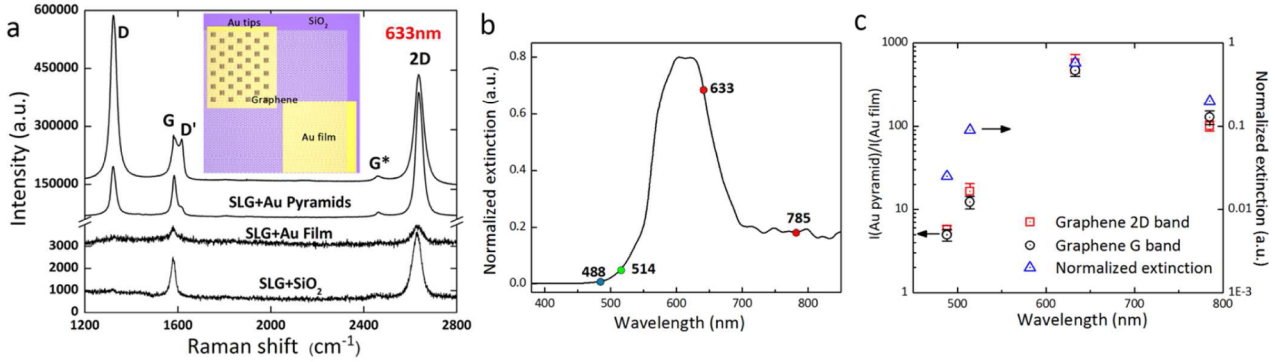

Figure 4. Raman spectra of single layer graphene (SLG) on Au tip structure and the wavelength selectivity. (a) Graphene Raman spectra measured from various surfaces (Au tips, flat Au, and SiO_2 as shown in the inset) with 633 nm excitation wavelength. (b) The extinction spectrum of Au tips, the three excitation wavelengths of 488, 514, 633, and 785 nm are marked with dots, respectively. (c) Ratios of intensity of graphene G and 2D peaks measured on the Au tip regions to those measured on flat Au regions, as well as normalized extinction at 4 wavelengths. The ratios in semilog scale are plotted as a function of the excitation wavelength.

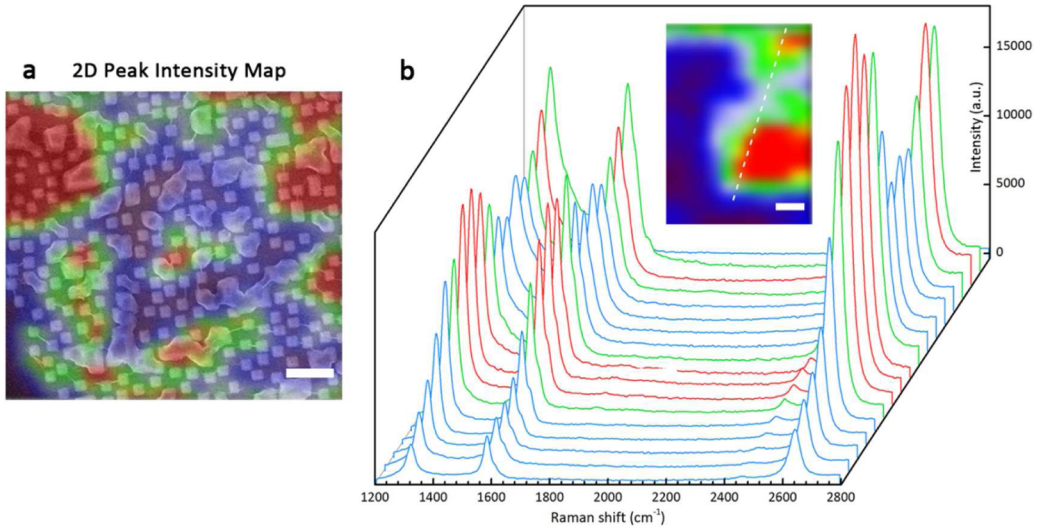

Figure 5. (a) Graphene 2D band intensity micro-Raman (633 nm) mapping data superimposed on the SEM image of the same region. Scale bar, 1 μm. (b) A series of Raman spectra from a line scan across a graphene SERS hotspot. The spectral interval is 200 nm. Scale bar, 500 nm.

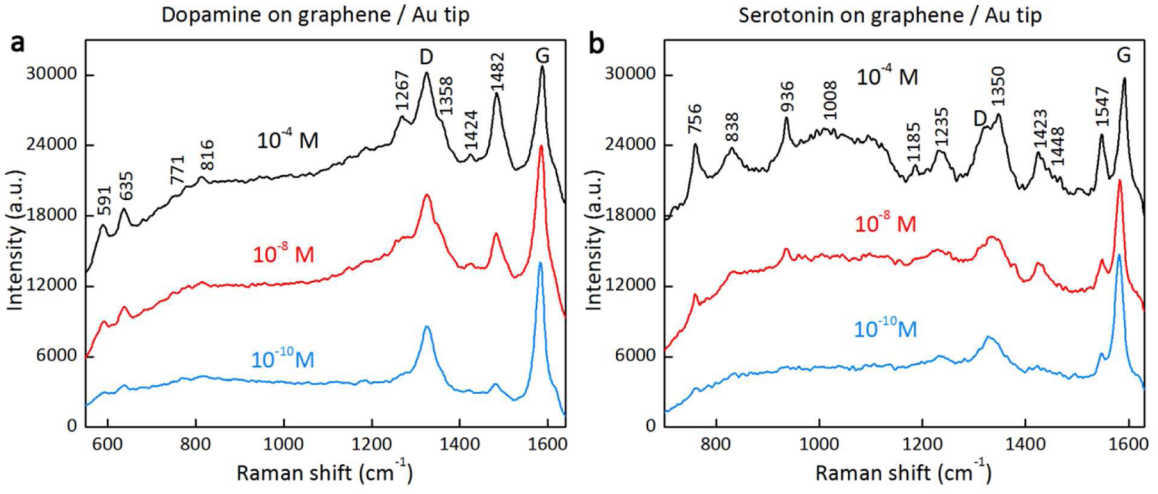

Figure 6. Raman spectra of neurotransmitter molecules on graphene hybrid structure with 3 different concentrations (10^{-4}, 10^{-8}, and 10^{-10} M). (a) Dopamine. (b) Serotonin. The laser excitation wavelength is 633 nm.

For the hybrid platform, the intensity of graphene SERS bands relates directly the local enhancement factor in the EM field.[24] The distribution of hot spots measured using spatially resolved graphene Raman mapping is shown in Figure 5. This way, the

DOI: 10.1021/acs.analchem.5b01560
Anal. Chem. 2015, 87, 10255−10261

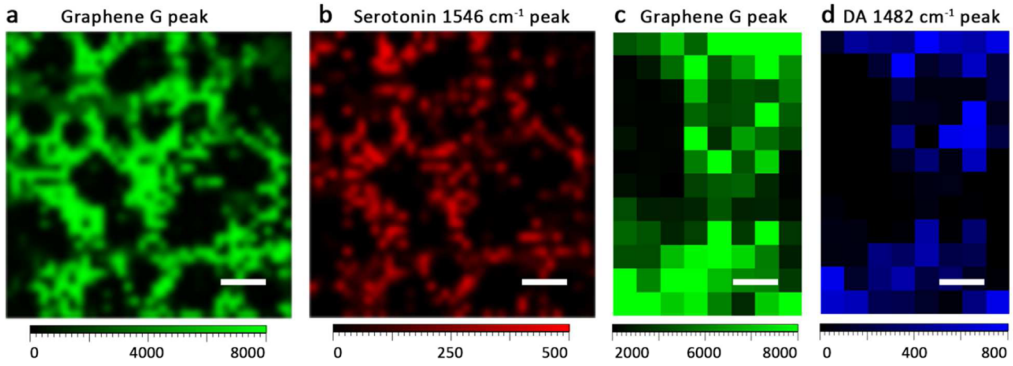

Figure 7. (a and b) Raman intensity mapping of graphene G band (green) and Raman intensity mapping of serotonin peak at 1546 cm^{-1} (red) of the same area, scale bar, 10 μm. (c and d) Raman intensity mapping of graphene G band (green) and Raman intensity mapping of dopamine peak at 1482 cm^{-1} (blue), scale bar, 2 μm.

hotspots where EM field is significantly increased could be precisely located using graphene SERS intensity mappings over the entire surface prior to performing measurements leading to significant reduction in the time required. The enhancement of the electric field of Au nanopyramids was modeled using finite-difference time-domain (FDTD) analysis, and the results were in good agreement with experimental results (see the Supporting Information).

Both SERS of dopamine and serotonin was achieved of concentration levels down to 10^{-10} M setting records in the label-free detection of the two important neurotransmitters. Figure 6a,b shows the average Raman intensities of dopamine and serotonin deposited on graphene−Au tip heterostructure at various molecular concentrations. The lowest concentration at which spectra can be unambiguously resolved is 10^{-10} M for both dopamine and serotonin. This value is the highest sensitivity ever reported in the literature to our knowledge.[25−27] Using the SERS EF definition proposed by Etchegoin,[28] we achieved the SERS EFs of dopamine and serotonin as 2×10^8 and 10^9, respectively (see the Supporting Information). We attribute the difference in SERS EFs to the chemical enhancement originated from the molecule−graphene interaction. The graphene layer on plasmonic structures could facilitate charge transfer between it and probe molecules, leading to an additional 10-times SERS intensity enhancement as shown by a previous study of ours.[23] Such chemical SERS enhancement, which we refer to as graphene-based enhanced Raman scattering (GERS), has been shown to be vibration mode dependent and particularly strong for selected Raman vibrations.[29] For example, the Raman peak for dopamine locates at 1482 cm^{-1}, which is assigned to phenyl C═C stretching mode[30] has a noticeably larger enhancement factor than the peaks assigned to other dopamine vibration modes. While for serotonin, the peaks located at 1423 and 1547 cm^{-1}, which are assigned to indole ring vibrations[31] have experienced the highest enhancement. Such preferential enhancement for ring related modes is believed to stem from chemical enhancement rendered by graphene.[32] The $\pi-\pi$ interactions between graphene and ring structures in dopamine as well as serotonin are believed to be a major contributing factor.[33,34] As shown in Figure 6, when the concentration is reduced to 10^{-10} M, the most easily recognized Raman peaks left are that of the 1482 cm^{-1} peak of dopamine and the 1423 and 1547 cm^{-1} peaks of serotonin.

As indicated in Figure 7a,b, the hotspots for the serotonin 1547 cm^{-1} peak and graphene G peak coincide with each other within the spatial resolution of micro-Raman. This feature can be appreciated by comparing their Raman intensity mappings over a large area. The colocation also exists for the dopamine 1482 cm^{-1} peak and graphene G peak. The direct correlation between molecule Raman peak intensity and graphene G-band intensity implies that the observed enhancements are due predominantly to EM enhancement.[35] This observation is of significance to the use of SERS for detecting trace amounts of target molecules. Such application is hindered in practice for most plasmonic structures due mainly to difficulties in locating hotspots. Hot spots over the VPMB platform can be precisely marked by graphene peak intensity mapping as discussed before thereby significantly reducing the time required during subsequent measurement of trace amount of target molecules.

A bianalyte SERS (BiASERS)[28,36,37] test of dopamine and serotonin has been conducted to establish single-molecule sensitivity of the VPMB platform (Figure 8). The BiASERS

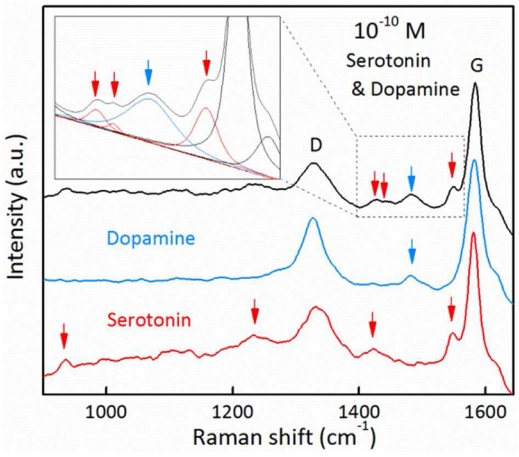

Figure 8. Raman spectra of 10^{-10} M serotonin and dopamine on heterostructure: Bianalyte mixed event: black. Dopamine single molecule event: blue. Serotonin single molecule event: red.

method is a contrast based spectroscopic technique that measures two different molecules at the same time. This approach facilitates reliable statistics based on a large spectral sample size for single molecule SERS detection. Aqueous solutions of dopamine and serotonin respectively of the same concentration are dispersed over VPMB platform. The frequency of both dopamine and serotonin SERS spectra being present at the same hot spot decrease monotonically with decreasing concentration. At 10^{-10} M level, we observed spectral response

DOI: 10.1021/acs.analchem.5b01560
Anal. Chem. 2015, 87, 10255−10261

from over 90% of SERS hot spots to be that of either dopamine or serotonin but not both thereby firmly establishing the single-molecule detection capability of VPMB for dopamine and serotonin.

To mimic the real biological environment with the interference from a variety of biomolecules (e.g., serum proteins) in the background,[38] we conducted SERS study of dopamine and serotonin dispersed in either cell culture medium (Dulbecco's modified Eagle's medium (DMEM) with 10% fetal bovine serum (FBS)) or simulated body fluids (SBF) with 10% FBS. Interference from background molecules blocks access to the hot spots with their relatively large molecular size. Such access hindrance has been shown to lead to signal degradation.[39,40] In our case, the sensitivity is reduced from the 10^{-10} M in water to 10^{-9} M in DMEM or SBF for both dopamine and serotonin (Figure 9). These results show that VPMB platform enables

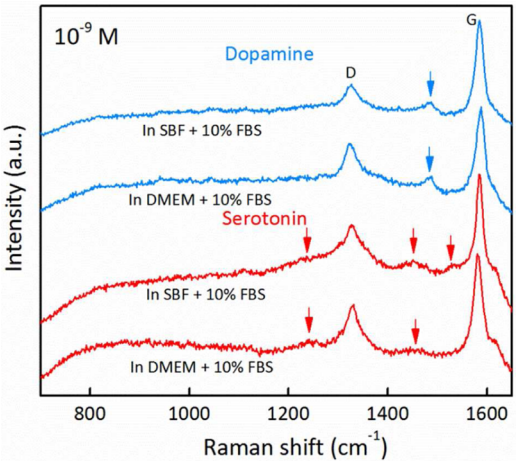

Figure 9. Raman spectra of 10^{-9} M dopamine (blue) and serotonin (red) dissolved in SBF supplemented with 10% FBS and DMEM supplemented with 10% FBS, respectively.

label-free detection of highly diluted dopamine and serotonin in simulated body fluid as encountered in a typical in vivo environment. Fe_3O_4/Ag nanocomposite system has been successfully applied to achieve selective dopamine SERS in artificial cerebrospinal fluid by surface modification.[41] The incorporation of similar techniques[41,42] with the hybrid platform holds the promise of becoming a highly useful tool for monitoring synaptic processes in vivo.

CONCLUSIONS

We demonstrate a graphene–plasmonic hybrid platform that allows us to detect dopamine and serotonin with a concentration as low as 10^{-9} M in simulated body fluid. Moreover, such sensitive detection is carried out in a label-free fashion with the copresence of both dopamine and serotonin. Such capability promises potential applications to the study of neurotransmitters in synaptic processes in vivo.

ASSOCIATED CONTENT

Supporting Information

The Supporting Information is available free of charge on the ACS Publications website at DOI: 10.1021/acs.analchem.5b01560.

Text, figures and tables giving the stability, reproducibility, repeatability test of the hybrid platform, the FDTD simulation of the EM field enhancement, the calculation of SERS EFs of dopamine and serotonin, and the SERS peak assignments of dopamine and serotonin (PDF)

AUTHOR INFORMATION

Corresponding Author

*Phone 1-310-825-2971. E-mail: yhx@ucla.edu.

Notes

The authors declare no competing financial interest.

ACKNOWLEDGMENTS

The authors acknowledge the support from Function Accelerated nanoMaterial Engineering (FAME) and California NanoSystems Institute (CNSI). P.W. and Y.H.X. would like to thank Prof. Yang Yang for granting us access to the Raman spectrometer. Y.H.X. acknowledges the support from Alexander von Humboldt Foundation Research Award that made this research possible.

REFERENCES

(1) Alivisatos, A. P.; Chun, M.; Church, G. M.; Greenspan, R. J.; Roukes, M. L.; Yuste, R. *Neuron* **2012**, *74*, 970–974.
(2) Zhang, A.; Neumeyer, J. L.; Baldessarini, R. J. *Chem. Rev.* **2007**, *107*, 274–302.
(3) Berger, M.; Gray, J. A.; Roth, B. L. *Annu. Rev. Med.* **2009**, *60*, 355–366.
(4) Ali, S. R.; Ma, Y.; Parajuli, R. R.; Balogun, Y.; Lai, W. Y.-C.; He, H. *Anal. Chem.* **2007**, *79*, 2583–2587.
(5) Carlsson, T.; Carta, M.; Muñoz, A.; Mattsson, B.; Winkler, C.; Kirik, D.; Björklund, A. *Brain* **2009**, *132*, 319–335.
(6) Politis, M.; Wu, K.; Loane, C.; Quinn, N. P.; Brooks, D. J.; Rehncrona, S.; Bjorklund, A.; Lindvall, O.; Piccini, P. *Sci. Transl. Med.* **2010**, *2*, 38ra46–38ra46.
(7) Fang, H.; Pajski, M. L.; Ross, A. E.; Venton, B. J. *Anal. Methods* **2013**, *5*, 2704–2711.
(8) Shankar, S. S.; Swamy, B.; Chandra, U.; Manjunatha, J.; Sherigara, B. *Int. J. Electrochem. Sci.* **2009**, *4*, 592–601.
(9) Tse, D. C.; McCreery, R. L.; Adams, R. N. *J. Med. Chem.* **1976**, *19*, 37–40.
(10) Anastassiou, C. A.; Patel, B. A.; Arundell, M.; Yeoman, M. S.; Parker, K. H.; O'Hare, D. *Anal. Chem.* **2006**, *78*, 6990–6998.
(11) Pande, S.; Jana, S.; Sinha, A. K.; Sarkar, S.; Basu, M.; Pradhan, M.; Pal, A.; Chowdhury, J.; Pal, T. *J. Phys. Chem. C* **2009**, *113*, 6989–7002.
(12) Liang, W.; He, S.; Fang, J. *Langmuir* **2014**, *30*, 805–811.
(13) Wang, Y.; Yan, B.; Chen, L. *Chem. Rev.* **2013**, *113*, 1391–1428.
(14) Abramczyk, H.; Brozek-Pluska, B. *Chem. Rev.* **2013**, *113*, 5766–5781.
(15) Jones, M. R.; Osberg, K. D.; Macfarlane, R. J.; Langille, M. R.; Mirkin, C. A. *Chem. Rev.* **2011**, *111*, 3736–3827.
(16) Xu, L.-J.; Zong, C.; Zheng, X.-S.; Hu, P.; Feng, J.-M.; Ren, B. *Anal. Chem.* **2014**, *86*, 2238–2245.
(17) Kaya, M.; Volkan, M. r. *Anal. Chem.* **2012**, *84*, 7729–7735.
(18) Wang, P.; Liang, O.; Zhang, W.; Schroeder, T.; Xie, Y. H. *Adv. Mater.* **2013**, *25*, 4918–4924.
(19) Hulteen, J. C.; Treichel, D. A.; Smith, M. T.; Duval, M. L.; Jensen, T. R.; Van Duyne, R. P. *J. Phys. Chem. B* **1999**, *103*, 3854–3863.
(20) Oh, J. R.; Moon, J. H.; Yoon, S.; Park, C. R.; Do, Y. R. *J. Mater. Chem.* **2011**, *21*, 14167–14172.
(21) Li, X.; Cai, W.; An, J.; Kim, S.; Nah, J.; Yang, D.; Piner, R.; Velamakanni, A.; Jung, I.; Tutuc, E. *Science* **2009**, *324*, 1312–1314.
(22) Sun, K.; Lee, J. Y.; Li, B.; Liu, W.; Miao, C.; Xie, Y.-H.; Wei, X.; Russell, T. P. *J. Appl. Phys.* **2010**, *108*, 036102–036104.
(23) Wang, P.; Zhang, W.; Liang, O.; Pantoja, M.; Katzer, J.; Schroeder, T.; Xie, Y.-H. *ACS Nano* **2012**, *6*, 6244–6249.
(24) Fang, Y.; Seong, N.-H.; Dlott, D. D. *Science* **2008**, *321*, 388–392.
(25) Bu, Y.; Lee, S. *ACS Appl. Mater. Interfaces* **2012**, *4*, 3923–3931.

DOI: 10.1021/acs.analchem.5b01560
Anal. Chem. 2015, 87, 10255–10261

(26) Zhao, J.; Zhang, W.; Sherrell, P.; Razal, J. M.; Huang, X.-F.; Minett, A. I.; Chen, J. *ACS Appl. Mater. Interfaces* **2012**, *4*, 44−48.
(27) Song, P.; Guo, X.; Pan, Y.; Wen, Y.; Zhang, Z.; Yang, H. *J. Electroanal. Chem.* **2013**, *688*, 384−391.
(28) Etchegoin, P. G.; Le Ru, E. C.; Fainstein, A. *Phys. Chem. Chem. Phys.* **2011**, *13*, 4500−4506.
(29) Ling, X.; Moura, L.; Pimenta, M. A.; Zhang, J. *J. Phys. Chem. C* **2012**, *116*, 25112−25118.
(30) An, J.-H.; El-Said, W. A.; Yea, C.-H.; Kim, T.-H.; Choi, J.-W. *J. Nanosci. Nanotechnol.* **2011**, *11*, 4424−4429.
(31) Tu, Q.; Eisen, J.; Chang, C. *J. Biomed. Opt.* **2010**, *15*, 020512−020513.
(32) Xu, W.; Ling, X.; Xiao, J.; Dresselhaus, M. S.; Kong, J.; Xu, H.; Liu, Z.; Zhang, J. *Proc. Natl. Acad. Sci. U. S. A.* **2012**, *109*, 9281−9286.
(33) Rochefort, A.; Wuest, J. D. *Langmuir* **2009**, *25*, 210−215.
(34) Uehara, Y.; Ushioda, S. *Appl. Phys. Lett.* **2005**, *86*, 181905.
(35) Campion, A.; Kambhampati, P. *Chem. Soc. Rev.* **1998**, *27*, 241−250.
(36) Le Ru, E.; Meyer, M.; Etchegoin, P. *J. Phys. Chem. B* **2006**, *110*, 1944−1948.
(37) Etchegoin, P. G.; Meyer, M.; Blackie, E.; Le Ru, E. C. *Anal. Chem.* **2007**, *79*, 8411−8415.
(38) Bonnier, F.; Knief, P.; Meade, A. D.; Dorney, J.; Bhattacharya, K.; Lyng, F. M.; Byrne, H. J. In *European Conferences on Biomedical Optics. Proc. SPIE* **2011**, 80870F−80870F-10.10.1117/12.889872
(39) Dieringer, J. A.; Lettan, R. B.; Scheidt, K. A.; Van Duyne, R. P. *J. Am. Chem. Soc.* **2007**, *129*, 16249−16256.
(40) Crozier, K. B.; Zhu, W.; Wang, D.; Lin, S.; Best, M. D.; Camden, J. P. *IEEE J. Sel. Top. Quantum Electron.* **2014**, *20*, 152−162.
(41) Ranc, V.; Markova, Z.; Hajduch, M.; Prucek, R.; Kvitek, L.; Kaslik, J.; Safarova, K.; Zboril, R. *Anal. Chem.* **2014**, *86*, 2939−2946.
(42) Balzerova, A.; Fargasova, A.; Markova, Z.; Ranc, V.; Zboril, R. *Anal. Chem.* **2014**, *86*, 11107−11114.

DOI: 10.1021/acs.analchem.5b01560
Anal. Chem. 2015, 87, 10255−10261